Short-range correlations and the 3s_{1/2} wave function in ^{206}Pb

M. R. Anders, S. Shlomo, and I. Talmi

Phys. Rev. C **92**, 034318 — Published 17 September 2015

DOI: 10.1103/PhysRevC.92.034318

Short range correlations and the $3s_{1/2}$ wave function in ^{206}Pb

M. R. Anders[1], S. Shlomo[1,2], and I. Talmi[2]

[1]Cyclotron Institute, Texas A&M University, College Station, Texas 77840

[2]The Weizmann Institute of Science, Rehovot 76100, Israel

Charge density difference between ^{206}Pb and ^{205}Tl, measured by elastic electron scattering, offers a unique opportunity to look for effects of short range correlations on a shell model wave function of a single proton. The measured difference is very similar to the charge density due to a proton in a $3s_{1/2}$ orbit. If there is a potential whose $3s_{1/2}$ wave function yields the measured difference between the charge distributions, no effect of short range correlations is evident. To check this point, we look for a potential whose $3s_{1/2}$ wave function yields the measured data. We developed a novel method to obtain the potential directly from the density and its first and second derivatives. Fits to parametrized potentials were also carried out. The $3s_{1/2}$ wave functions of the potentials determined here, reproduce fairly well the experimental data within the quoted errors. To detect possible effects of two-body correlations on the $3s_{1/2}$ shell model wave function, more accurate measurements are required.

PACS numbers: 21.60.Cs, 30.Bf, 21.10.Gv, 27.80.+w

1. Introduction

An important problem is how the success of the nuclear shell model can be reconciled with the strong and short ranged interaction between free nucleons. It was realized that shell model wave functions are eigenstates of a *renormalized* nuclear Hamiltonian in which the interactions are rather tame. Thus, shell model wave functions, of independently moving nucleons, do not have short range correlations. The latter are imposed on the *real* wave functions by the strong short-range interaction between free nucleons (the bare interaction). According to current results of the nuclear many-body theory, short-range two-nucleon correlations due to the bare interaction, play an important role. In some papers, the admixtures into shell model wave functions due to correlations were calculated to be rather high, up to 35% [1,2].

Still, there are indications that shell model wave functions have a certain reality. A possible way to check it was to measure the difference between charge distributions of two nuclei with the same N and Z_2=Z_1-1 [3]. A much higher accuracy was obtained by Frois et al [4,5] who measured the difference between the charge densities of ^{206}Pb and ^{205}Tl. The authors used elastic electron scattering. The difference between the charge distributions which they determined is very similar to the one due to a proton wave function in a $3s_{1/2}$ orbit. It has a clear maximum at the origin and two additional maxima. This result is in agreement with the simple shell model. The $½^+$ ground state of ^{205}Tl shows that the $3s_{1/2}$ orbit is the highest in the proton Z=82 major shell. The authors noticed that the experimental charge density near r = 0 is much lower than the one due to a Hartree-Fock calculation and to the one obtained from a conventional Wood-Saxon single particle potential. They attributed it to a rather strong (30%) admixture of a shell model wave function in which the proton hole is in a $2d_{3/2}$ state, coupled to a J=2 state of two neutron holes [4,5]. As pointed in Ref. [6], the inclusion of the $2d_{3/2}$ orbital leads to an agreement with data at the origin but deviations from data by a factor of two occur in the region between 2 to 4 fm. An attempt to obtain the observed shape of the charge distribution from a conventional Wood-Saxon potential was carried out in Ref. [6]. The authors assumed a significant modification of the proton form factor (increasing the charge radius) in medium. This assumption was also made to explain the EMC effect. However, it was shown in Ref. [7] that the EMC effect was simply explained by the fact that nucleons are bound in a nucleus. One should use the four momenta distribution function in calculating the deep inelastic muon (electron) cross section on a nucleus.

A large deviation from the shell model wave function has direct implications to direct nuclear reactions. Results of these reactions depend on the occupation probability of shell model orbits. The estimates obtained by analysis of experimental data are usually less than those expected from the shell model. Such estimates are based on measured cross sections of various reactions which seem to be smaller than those calculated with shell model wave functions. Unlike the depletions which are considered in those reactions, the measured ^{206}Pb - ^{205}Tl charge difference is *exactly* equal to 1 proton charge. Any effect of short range correlations could only modify the *shape* of the difference between the charge distributions. The striking results of the measured difference of the charge densities [4,5] deserve attention. In the present paper, we look for a potential whose proton $3s_{1/2}$ wave function can reproduce the measured difference.

If such a potential exists, no effect of short range correlations is evident in the experimental data. This would definitely not contradict the existence of those correlations. The latter cause "wounds" in shell model wave functions. If the wound occupies a small volume, it will not have a big effect on expectation values of "long range" operators. This term was used in a paper on *ab initio* calculations [8]. The authors consider short range and long range operators. They find that "when the operator becomes long range, the renormalized operator becomes indistinguishable from the bare value". This means that for long range operators, shell model wave functions may be safely used.

If a potential as described above is found, it could serve also as an additional constraint in the determination of a modern energy density functional (EDF) for more reliable prediction of properties of nuclei and nuclear matter [9,10].

We developed a new method to determine the single particle potential directly from the single particle matter density and its first and second derivatives. In section 2 we consider the single particle Schrodinger equation and describe the method for determining the single particle potential $V(\vec{r})$ from a given single particle wave function $\psi(\vec{r})$ or matter density, $\rho(\vec{r})$, assuming it is known for all $\vec{r}$. In particular, we consider the case of spherical symmetry. We also describe the method of deducing the point proton density directly from the charge distribution determined in electron scattering measurements. In section 3 we present our attempts to construct a single nucleon potential whose $3s_{1/2}$ proton wave function yields a good fit to the data. The experimental data [4,5] is for the charge density difference between the close $(\Delta Z = 1)$ isotones ^{206}Pb – ^{205}Tl. In Section 4 we present our conclusions.

2. Formalism

Consider the single particle Schrodinger equation,

$$-\frac{\hbar^2}{2m}\Delta\psi + V\psi = E\psi \ , \tag{1}$$

where $V(\vec{r})$ is a real local and non-singular potential. From Eq. (1) follows that for a given single particle wave function $\psi(\vec{r})$, known for all $\vec{r}$, and given eigenvalue *E,* the corresponding single particle potential *V* is uniquely determined by

$$V(\vec{r}) = E + \frac{\hbar^2}{2m}S(\vec{r}), \qquad S(\vec{r}) = \frac{\Delta\psi(\vec{r})}{\psi(\vec{r})}. \tag{2}$$

For a non-singular *V*, $\Delta\psi(\vec{r}) = 0$ when $\psi(\vec{r}) = 0$. The relation for $[\psi(\vec{r})]^b$, where b is a positive integer, is given in Ref. [11]. In the present paper we consider the spherically symmetric case where,

$$\psi_{nlj}(\vec{r}) = \frac{R_{nlj}(r)}{r}Y_{lj} \ . \tag{3}$$

Here, $R_{nlj}(r)$ is the radial wave function for the orbit with principal number *n*, orbital angular momentum *l* and total angular momentum *j* and Y_{lj} is the eigenfunction of the angular momenta *l* and *j*. In the following we limit the discussion to the proton $3s_{1/2}$ orbit. Therefore, the corresponding single particle potential for a nucleon is

$$V_{cen}(r) = E + \frac{\hbar^2}{2m}S(r) - \frac{1}{2}(1-\tau_z)V_{coul}(r), \qquad S(r) = \frac{1}{R_{nlj}(r)}\frac{d^2R_{nlj}}{dr^2} \ . \tag{4}$$

where $V_{cen}(r)$ and $\frac{1}{2}(1-\tau_z)V_{coul}(r)$, are the central and coulomb potentials, respectively. Here, τ_z=1 for a neutron and -1 for a proton.

The single particle radial density $\rho_{nlj}(r)$ is related to the square of the radial wave function R^2_{nlj} by

$$R^2_{nlj}(r) = 4\pi r^2 \rho_{nlj}(r)\ . \tag{5}$$

From (5) it is possible to extract the wave function $R_{nlj}(r)$ and use Eq. (4) to deduce the corresponding single particle potential, but this leads to additional complications. Therefore, we developed a method to determine the potential directly from the density and
second derivatives. Using Eq. (4), we obtain the simple relation with R^2_{nlj},

$$S(r) = \frac{1}{2R^2_{nlj}}\left[\frac{d^2(R^2_{nlj})}{dr^2} - \frac{1}{2}\frac{1}{R^2_{nlj}}\left[\frac{d(R^2_{nlj})}{dr}\right]^2\right]. \tag{6}$$

When $R^2_{nlj} = 0$, $dR^2_{nlj}/dr = 0$ with the additional condition that the term on the right hand side (r.h.s) of Eq. (6) in the square brackets also vanishes. From Eqs. (5) and (6) we find the relation,

$$S(r) = \frac{1}{2\rho_{nlj}}\left[\frac{d^2\rho_{nlj}}{dr^2} + \frac{2}{r}\frac{d\rho_{nlj}}{dr} - \frac{1}{2\rho_{nlj}}\left(\frac{d\rho_{nlj}}{dr}\right)^2\right]. \tag{7}$$

When $\rho_{nlj} = 0$, $d\rho_{nlj}/dr = 0$ with the additional condition that the term $\frac{d^2\rho_{nlj}}{dr^2}$ also vanishes.

A commonly used central nuclear potential is the Woods Saxon (WS) potential,

$$V(r) = V_0/[1 + exp((r - R_1)/\mathrm{a}_0)]\ , \tag{8}$$

where, V_0, R_1 and a_0 are the depth, half radius and diffuseness parameters, respectively. For the Coulomb potential we adopt the form obtained from a uniform charge distribution of radius R_{ch},

$$V_{coul}(r) = Ze^2\begin{cases}(3 - r^2/R^2_{ch})/2R_{ch} & r < R_{ch}\\ 1/r & r > R_{ch}\end{cases}\ , \tag{9}$$

with $R^2_{ch} = (5/3)\langle r^2\rangle_{ch}$, where $\langle r^2\rangle_{ch}$ is the charge mean square radius.

In elastic electron-nucleus scattering measurements the charge density distribution, $\rho_{ch}(\vec{r})$, is determined by carrying out a phase shift analysis of the cross section [12]. In theoretical models the point proton density distribution, $\rho_p(\vec{r})$ is calculated. The difference between the two distributions is due to the finite size of the proton internal charge distribution. They are related by the convolution relation

$$\rho_{ch}(\vec{r}) = \int \rho_p(\vec{r'})\,\rho_{pfs}(\vec{r} - \vec{r'})d^3\vec{r'}\ , \tag{10}$$

where $\rho_{pfs}(\vec{r})$ is the charge density distribution of the proton. The experimental elastic electron scattering data of a free proton can be well reproduced by the expression

$$\rho_{pfs}(r) = \frac{1}{8\pi a^3}e^{-r/a}\ , \tag{11}$$

where $a^2 = \frac{1}{12}r^2_{pfs}$ with $r_{pfs} = 0.85$ fm being the corresponding charge root mean square (rms) radius [12,13]. The Fourier transform of the charge density $\rho_{ch}(\vec{r})$, determined by the convolution relation of Eq. (10) is given by

$$F_{ch}(q) = F_{pfs}(q)F_p(q)\ , \tag{12}$$

where $F_{ch}(q)$, $F_{pfs}(q)$ and $F_p(q)$, are the Fourier transfoms of $\rho_{ch}(\vec{r})$, $\rho_{pfs}(\vec{r})$ and $\rho_p(\vec{r})$, respectively. Eq. (12) can be used to determine the form factor $F_p(q)$, associated with the point proton density distribution $\rho_p(r)$. Then $\rho_p(r)$ can be obtained from $F_p(q)$ by the inverse Fourier transform and compared with theoretical predictions.

3. Results

In Fig. 1a we present (solid line) the experimental data [4,5] for the charge density difference, $\Delta\rho_c(r) = \rho_c(r;\ ^{206}\mathrm{Pb}) - \rho_c(r;\ ^{205}\mathrm{Tl})$, between the isotones ^{206}Pb – ^{205}Tl. It is normalized by the charge of one proton (Z=1) and hence, it is replaced in the following, by 1. The dotted lines indicate the limits of experimental uncertainty. The two maxima like those of the proton $3s_{1/2}$ orbit are clearly seen in the Figure. The

experimental values of the charge rms radii of ^{206}Pb and ^{205}Tl are 5.4897 and 5.4792 fm, respectively, leading to a value of 6.2822 fm for the charge rms radius of the proton $3s_{1/2}$ orbit. To assess the possible rearrangement effect (from ^{205}Tl to ^{206}Pb) on the charge rms radius of the 81 core protons in ^{206}Pb, we assume that it increases by 0.005 fm, similar to the change between ^{206}Pb and ^{207}Pb [3]. The rearrangement effect is approximated (see Ref. [3]) by scaling the charge distribution of ^{205}Tl so that the charge rms radius of the scaled density is equal to that of the 81 core protons in ^{206}Pb. We thus obtain

$$\Delta\rho_{Rc}(r) = \rho_c(r;\ ^{206}\text{Pb}) - \alpha^3\rho_c(\alpha r;\ ^{205}\text{Tl}), \qquad (13)$$

where the scaling parameter α = 5.4792/(5.4792 + 0.005) = 0.9990 is the ratio between the charge rms radius of ^{205}Tl to that of the core 81 protons in ^{206}Pb. The form of (13) guarantees that the integral of $\Delta\rho_{Rc}(r)$ is equal to 1. The results for the charge density $\Delta\rho_{Rc}(r)$ are shown in Figure 1a (dashed line).

To extract the corresponding single particle potential, using Eqs. (4) and (6) or (7), we need the point proton distribution, $\Delta\rho_p(r)$. It is obtained by using Eqs. (11) and (12) to determine the point proton form factor, $F_p(q)$, and then obtain $\Delta\rho_p(r)$ by inverse Fourier transform. Using the relation (5) we determined the values of $R_p^2(r) = 4\pi r^2\Delta\rho_p(r)$ as obtained from Figure 1a and shown by the solid line in Figure 1b. If $\Delta\rho_p(r)$ is obtained from an eigenfunction of Eq.(1), $R_p(r)$ is related to it by (5). Similarly, $R_{Rp}^2(r) = 4\pi r^2\Delta\rho_{Rp}(r)$. The dashed line in Figure 1b, is obtained from the dashed line in Figure 1a. The dotted lines indicate the experimental uncertainty. We note that $R_p^2(r)$ as obtained from Figure 1a (solid line) is slightly negative at the first node (at ~ 2.6 fm) and above zero at the second node (r ~ 4.9 fm). In Refs. [4,5] it was concluded that this result is consistent with the proton $3s_{1/2}$ orbit in the vicinity of these minima. however, the experimental uncertainty in $R_p^2(r)$ is larger than its value. The magnitude of the difference between $\Delta\rho_p(r)$ and $\Delta\rho_{Rp}(r)$ is similar to that of the experimental uncertainty.

We tried to use the experimental $R_p^2(r)$ and $R_{Rp}^2(r)$ of Figure 1b, shown by the solid and dashed lines, respectively, to directly deduce the corresponding potentials by employing (4) and (6). The Coulomb potential of Eq. (9), with $R_{ch} = 7.1$ fm, was adopted in the calculations. For non-singular potential V, the second derivative $\frac{d^2R}{dr^2}$ should vanish when $R(r) = 0$. As seen from Figure 1b, this condition is not fulfilled at the minima of the experimental $R_p^2(r)$. Moreover, in the vicinity of the minima, in the regions of r = 2.0 – 3.0 fm and r = 4.5 – 5.5 fm, the uncertainty in $\Delta\rho_p(r)$ is larger than 50% of its value. Due to the large uncertainties in the experimental data, no reliable potential can be extracted.

Therefore, we considered several nuclear central potentials with the given Coulomb potential (9) added to each. We looked for potentials whose $3s_{1/2}$ wave functions yield charge distributions which fit best the measured one. The parameters of these potentials are obtained by least squares fits of the calculated $R_p^2(r)$ to the corresponding experimental data. The fitted potential $V_F(r)$ is obtained by taking the values of the potential at the points r = 3, 6 and 9 fm as free parameters. The value of $V_F(0)$ is constrained to reproduce the experimental value of 7.25 MeV for the separation energy of the proton in the $3s_{1/2}$ orbit of ^{206}Pb. The value of $V_F(12)$ is taken to be zero. The values of $V_F(r)$ between these points are determined by polynomial interpolation (solid line in Fig.2). From a fit to the experimental data of $R_p^2(r)$, solid line in Figure 1b, we obtained the values of the parameters of $V_F(r)$ given in Table 1. Similarly, the potential $V_{RF}(r)$ (dashed line) is obtained by a fit to $R_{Rp}^2(r)$ (dashed line in Figure 1b), with values of the parameters shown in Table 1. The potential $V_{WSF}(r)$, dashed double dotted line, is obtained by fitting the Wood-Saxon potential (8) to $R_p^2(r)$. The values of its parameters are given in Table 1. For comparison, a conventional Wood-Saxon potential $V_{WS}(r)$ is also shown, by the dashed-dotted line, with the values of its parameters given in Table 1.

In Figures 3a and 3b, the experimental data of $R_c^2(r) = 4\pi r^2\Delta\rho_c(r)$ and of $\Delta\rho_c(r)$ (between the two dotted lines) are compared with results of the proton $3s_{½}$ orbit. The latter were obtained from the potentials described above, and shown in Figure 2. The agreement between the experimental values and the results of the fitted $V_F(r)$ potential (solid line) is fair with χ^2/N = 1.15. The results of the potential V_{RF}(r) (not sown in Figure 3) are also in fair agreement with the data, χ^2/N = 1.81. The results of the fitted potential V_{WSF}(r), (dashed double dotted line) are also in reasonable agreement with the data, χ^2 /N=

3.28. For comparison, we also show by the dashed-dotted line the results of the conventional Wood Saxon potential $V_{WS\backslash}(r)$. The agreement is much poorer, with the value of $\chi^2/N = 8.85$.

The potential well of the shell model may well depend on the mass number A. It may also be non-local and depend on l. Still, it is interesting to look at the charge distribution due to the proton s-orbits occupied in ^{206}Pb. They are the only orbits which contribute to the point proton density distribution at r=0. In Figures 4a, b and c we compare the charge density of the $1s_{1/2}$, $2s_{1/2}$ and $3s_{1/2}$ proton orbits, respectively, obtained from the fitted potential $V_F(r)$ (solid lines) with those obtained from the conventional Wood-Saxon potential $V_{WS}(r)$ (dashed-double dotted line). The calculated contribution to $\rho_{ch}(0)$ of the $s_{1/2}$ proton orbits for the fitted potential $V_F(r)$ is 0.053 fm^{-3}, significantly smaller than the value of 0.073 fm^{-3} obtained from the conventional Wood-Saxon potential, $V_{WS}(r)$, leading to a better agreement with the experimental observation of $\rho_{ch}(0) = 0.063$ for ^{206}Pb [4,5,13]. The separation energies of the $1s_{1/2}$, $2s_{1/2}$ and $3s_{1/2}$ proton orbits are -47.09, -22.64 and -7.24 MeV for the $V_F(r)$ potential and -36.31, -24.46 and -8.00 MeV for the $V_{WS}(r)$ potential, respectively. The relatively large separation energy of the $1s_{1/2}$ proton orbit obtained for the $V_F(r)$ is close to the experimental value of -64.8 MeV [14].

4. Conclusion

The difference between the charge distributions of ^{206}Pb and ^{205}Tl was measured many years ago. It offers a good opportunity to study possible effects of short range correlations on the shell model wave function of a proton in the $3s_{1/2}$ orbit. Effects of this kind were estimated by comparing measured cross sections of various reactions to those calculated using shell model wave functions. Usually, the measured values were lower than the calculated ones. This depletion was sometimes attributed to effects of short range correlations. The difference between the charge distributions considered here, cannot be depleted. The integrated difference between charge densities must be exactly equal to the charge difference between the two isotones, 1 proton charge. The effects of short range correlations in this case can only change the *shape* of the difference between the charge distributions.

The experimental values of that difference have features which are very similar to those due to the wave function of a proton in some $3s_{1/2}$ orbit. These are two zero values for $r > 0$ which correspond to the two nodes of the 3s wave function $R(r)/r$. If the point proton distribution $\rho_p(r)$ is due to a 3s wave function, two conditions should be satisfied, in addition to its having first and second derivatives for all r values. These conditions are presented after Eq. (7). They are necessary to derive the single nucleon potential, using (4), (6) or (7) from a proton distribution $\rho_p(r)$. It is difficult to see whether these conditions are satisfied by the measured difference of charge distributions. The experimental accuracy is not sufficient, particularly near the zero values.

We started by deriving and employing a new relation [11] between the potential V and the single particle density and its first and second derivatives. Due to insufficient experimental accuracy, no reliable potential can be obtained in this way. In view of this situation, we tried to construct nuclear single particle potential V whose proton $3s_{1/2}$ orbit in ^{206}Pb yield charge distributions which best fit the electron scattering results [4,5]. We found several potentials which yield fair fits to the data (Fig. 3). The fair agreement with fitted potentials may be an indication that effects of short range correlations on charge distributions of shell model wave functions are not significant. Still, to answer the question to what extent the data agree with the distribution due to a 3s wave function of some potential, better accuracy of the measurement is needed. The uncertainty in values of $\Delta\rho_c(r)$ must be reduced by a factor of two or more before an accurate determination of the effects of short range correlations on shell model wave functions can be achieved. This is a strong demand on the plan of experiments described in Ref. [15].

S. S. would like thank The Weizmann Institute of Science for the kind hospitality. This work was supported in part by US Department of Energy under Grant No. DOE-FG03-93ER40773. .

[1] N. Antonov, P. E. Hodgson and I. Zh. Petkov, *Nucleon Momentum and Density Distributions in Nuclei* (Clarendom Press, Oxford, 1988); *Nucleon Correlations in Nuclei* (Springer-Verlag, berlin/Heidelberg/New York, 1993).
[2] V. R. Pandharipande, I. Sick and P. K. A. deWitt Huberts, Rev. Mod. Phys. **69**, 961 (1997).
[3] H. Euteneuer, J. Friedrich and N. Voegler, Nucl. Phys. **A298**, 452 (1978).
[4] J. M. Cavedon, *et al*, Phys. Rev. Lett.**49**, 978(1982).
[5] B. Frois, et al, Nucl. Phys. **A396**, 409c (1983).
[6] L. S. Celenza, A. Harindranath, and C. M. Shakin, Phys. Rev. C **32**, 2173 (1985).
[7] S. V. Akulinichev, S. Shlomo, S. A. Kulagin and G. M. Vagradov, Phys. Rev. Lett. **55**, 2239 (1985).
[8] I Stetcu, B.R.Barrett, P.Navratil, and J.P.Vary, Phys.Rev. C **71,** 044325 (2005).
[9] S. Shlomo, in *The Universe Evolution: Astrophysical and Nuclear Aspects,"* Eds., L. Blokhintsev and I. Strakovsky, Nova Science Publishers, 2013.
[10] B. K. Agrawal, S. Shlomo and V. Kim Au, Phys. Rev. C **72**, 014310 (2005).
[11] M. R. Anders, et al, to be published.
[12] L. R. B. Elton, *Nuclear Sizes*, Oxford University Press, London, 1961.
[13] H. De Vries, C. W. De Jager, and C. de Vries, Atomic Data an Nuclear Data Tables **36**, 495 (1987).
[14] A. A. Vorobev, Y. V. Dotsenko, A. A. Lobodenko, O. V. Miklukho, I. I. Tkach, A. Y. Tsaregorodtsev, and Y. A. Shcheglov, Phys. At. Nucl. **58**, 1817 (1995).
[15] A. N. Antonov, *et* al., Nuclear Instrument and Methods in Physics Research A **637**, 60 (2011).

Table 1. Values of parameters of standard Woods Saxon (WS) potential and the fitted potentials.

	V_{WS}	V_{WSF}	V_F	V_{RF}
χ^2/N	8.85	3.28	1.15	1.81
V_0 [MeV]	-62.712	-167.95		
R_1 [fm]	7.087	-0.03		
a_0 [fm]	0.65	4.68		
$V(0)$ [MeV]			-58.19	-51.33
$V(3)$ [MeV]			-81.35	-88.29
$V(6)$ [MeV]			-34.50	-33.64
$V(9)$ [MeV]			-23.54	-23.96
$V(12)$ [MeV]			0.00	0.00

FIGURE CAPTIONS

Fig.1(a) The experimental difference, $\Delta\rho_c(r)$ between ^{206}Pb and ^{205}Tl charge distributions (solid line). The dashed line is for $\Delta\rho_{Rc}(r)$, the data after rearrangement correction. The dotted lines indicate the experimental uncertainty. (b) Similar to (a) for $R_P^2(r) = 4\pi r^2 \Delta\rho_p(r)$ where $\Delta\rho_p(r)$ is derived from the experimental $\Delta\rho_c(r)$. The dashed line is for $R_{Rp}^2(r)$ related to $\Delta\rho_{Rp}(r)$ similarly obtained from $\Delta\rho_{Rc}(r)$.

Fig.2 Potentials fitted to data in Fig.1b. The $V_F(r)$ potential (solid line), the $V_{FR}(r)$ version including rearrangement (dashed line) and the fitted $V_{FWS}(r)$ potential (double dotted-dashed line). Also shown is the conventional Wood-Saxon $V_{WS}(r)$ potential (dashed-dotted line).

Fig.3 Experimental values of $R_c^2(r) = 4\pi r^2 \Delta\rho_c(r)$ (a) and $\Delta\rho_c(r)$ (b) plotted between dotted lines of error limits. They are compared to calculated charge distributions due to the $3s_{1/2}$ wave functions of the fitted $V_F(r)$ potential (solid lines), the fitted Wood-Saxon $V_{FWS}(r)$ potential (double dotted-dashed lines) and the conventional $V_{WS}(r)$ potential (dashed-dotted lines.

Fig.4 Calculated charge densities of a proton in the $1s_{1/2}$ (a), $2s_{1/2}$ (b) and $3s_{1/2}$ (c) orbits in the $V_F(r)$ potential (solid lines) and the conventional $V_{WS}(r)$ potential (double dotted-dashed lines).

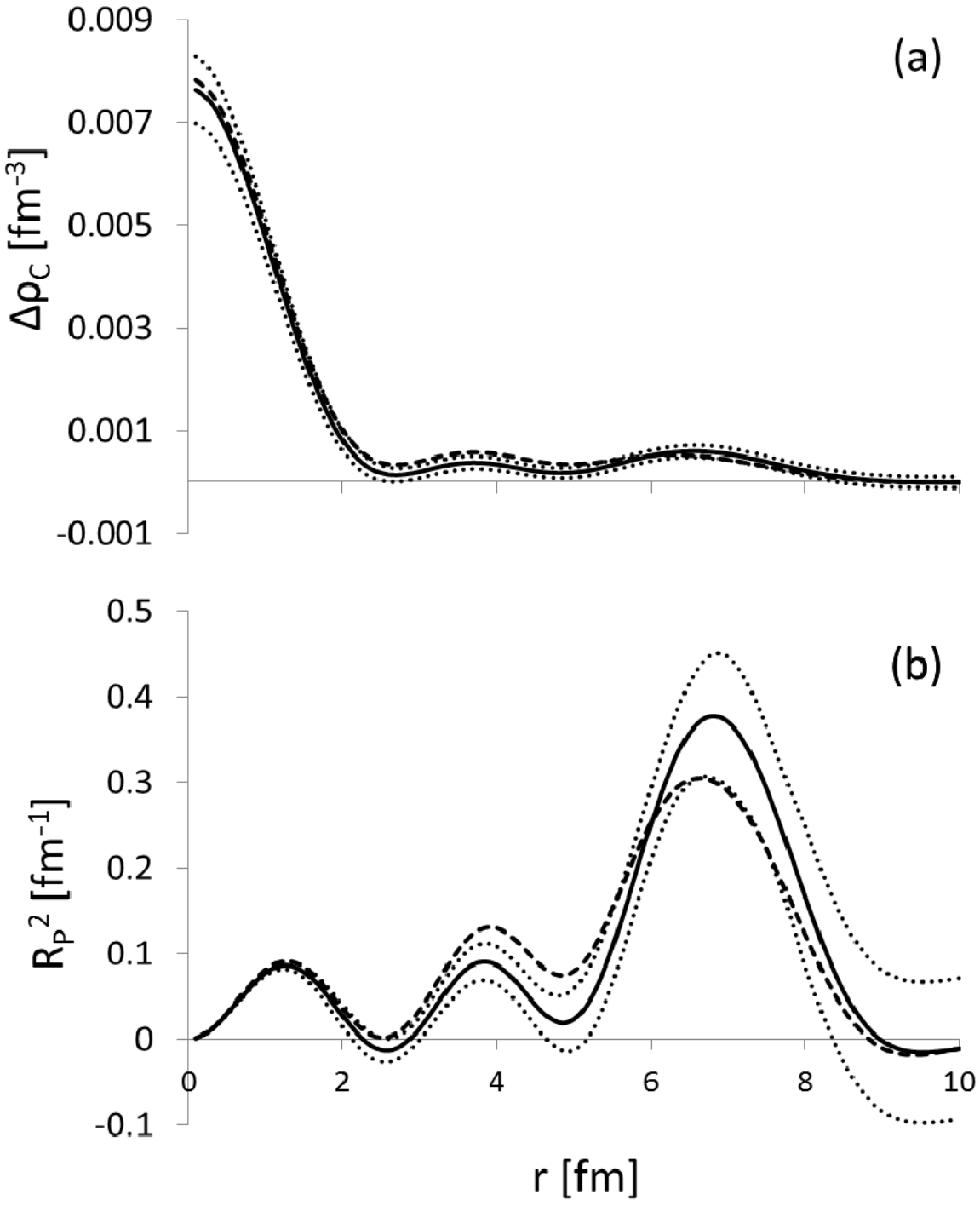

Fig.1(a) The experimental difference, $\Delta\rho_c(r)$ between ^{206}Pb and ^{205}Tl charge distributions (solid line). The dashed line is for $\Delta\rho_{Rc}(r)$, the data after rearrangement correction. The dotted lines indicate the experimental uncertainty. (b) Similar to (a) for $\Delta\rho_p(r)$ where $\Delta\rho_p(r)$ is derived from the experimental $\Delta\rho_c(r)$. The dashed line is for related to $\Delta\rho_{Rp}(r)$ similarly obtained from $\Delta\rho_{Rc}(r)$.

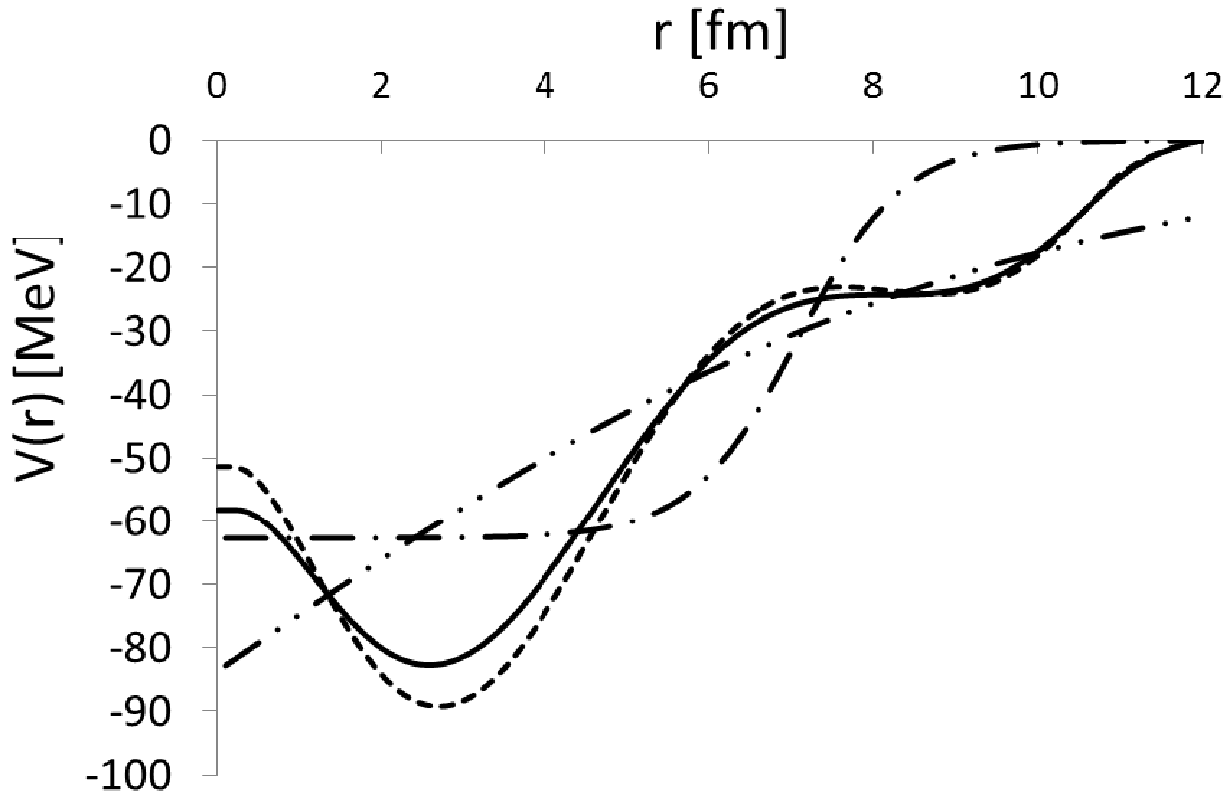

Fig.2 Potentials fitted to data in Fig.1(b). The $V_F(r)$ potential (solid line), the $V_{FR}(r)$ version including rearrangement (dashed line) and the fitted $V_{FWS}(r)$ potential (double dotted-dashed line). Also shown is the conventional Wood-Saxon $V_{WS}(r)$ potential (dashed-dotted line).

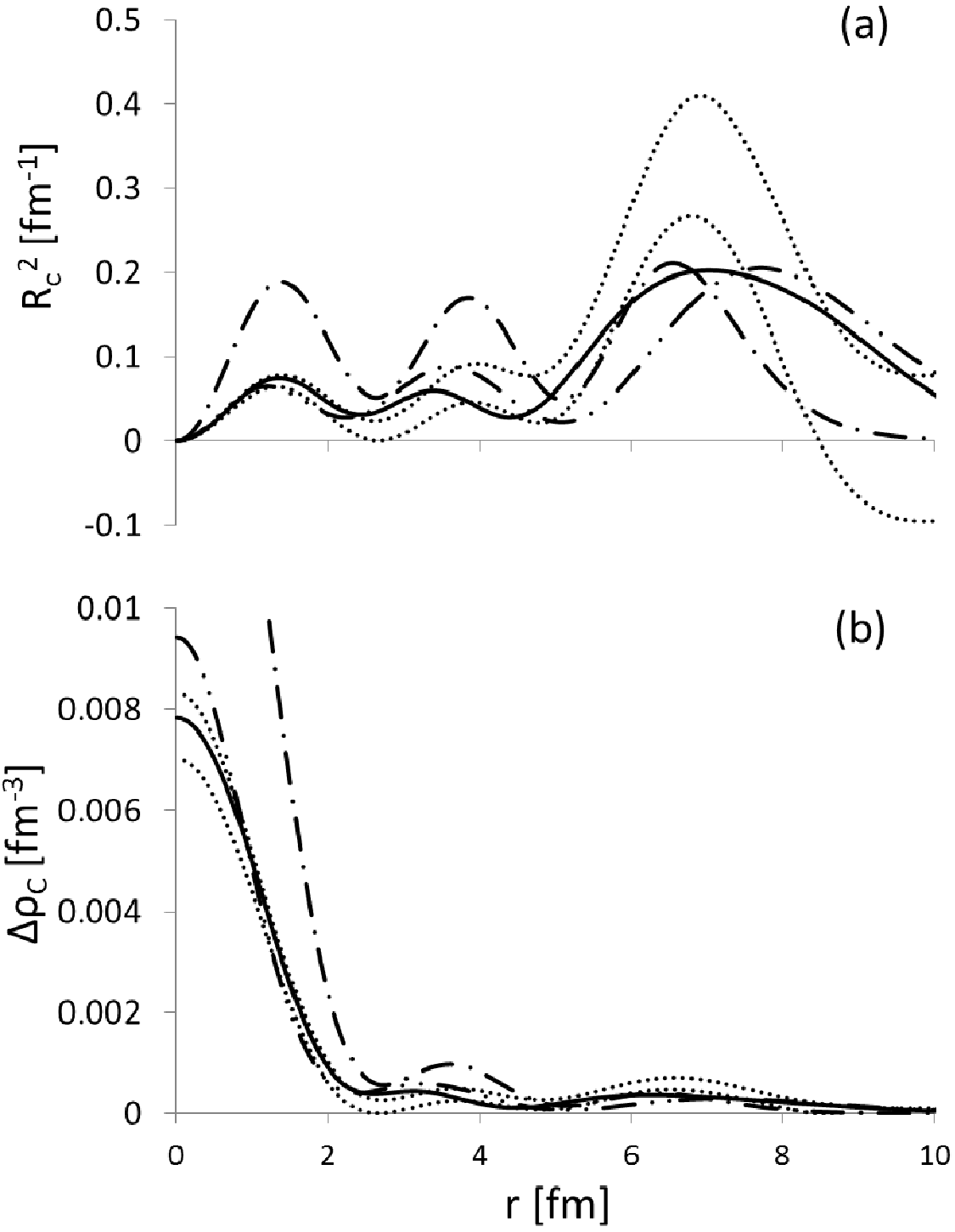

Fig.3 Experimental values of (a) and (b) plotted between dotted lines of error limits. They are compared to calculated charge distributions due to the $3s_{1/2}$ wave functions of the fitted $V_F(r)$ potential (solid lines), the fitted Wood-Saxon $V_{FWS}(r)$ potential (double dotted-dashed lines) and the conventional $V_{WS}(r)$ potential (dashed-dotted lines.

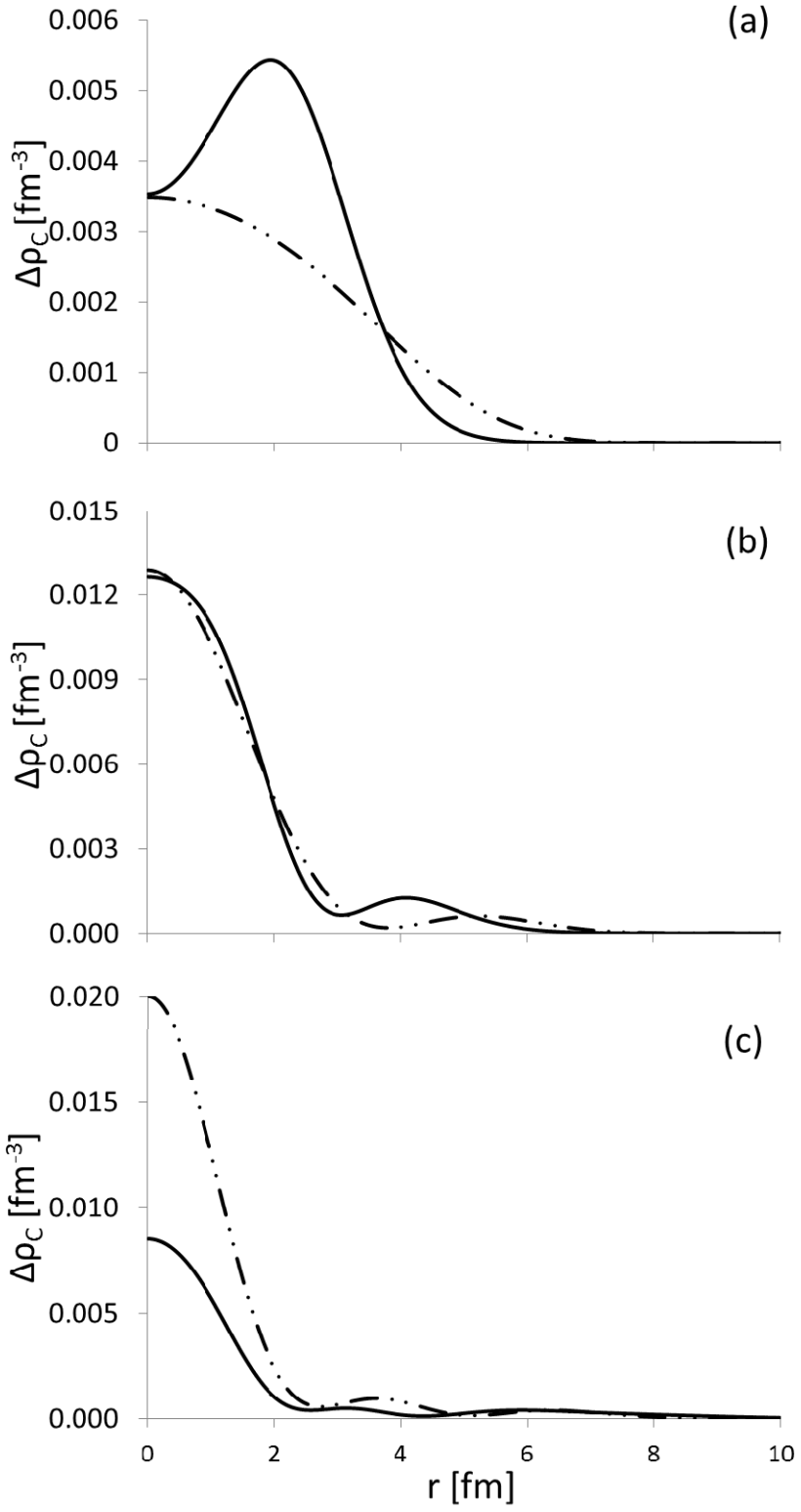

Fig.4 Calculated charge densities of a proton in the $1s_{1/2}$ (a), $2s_{1/2}$ (b) and $3s_{1/2}$ (c) orbits in the $V_F(r)$ potential (solid lines) and the conventional $V_{WS}(r)$ potential (double dotted-dashed lines).